physica status solidi (a)

RESEARCH ARTICLE OPEN ACCESS

Irradiation-Resistant Heterostructures Based on Monolayer MoS_2

Emanuele Sangiorgi[1] | Francesca Migliore[1] | Antonino Madonia[1] | Antonino Alessi[1,2] | Romain Grasset[2] | Olivier Cavani[2] | Salvatore Ethan Panasci[3] | Emanuela Schilirò[3] | Filippo Giannazzo[3] | Fiorenza Esposito[4,5] | Luca Seravalli[4] | Marco Cannas[1] | Simonpietro Agnello[1,6]

[1]Department of Physics and Chemistry Emilio Segrè, University of Palermo, Palermo, Italy | [2]LSI, CEA/DRF/IRAMIS, CNRS, Ecole Polytechnique, Institut Polytechnique de Paris, Palaiseau, France | [3]Consiglio Nazionale delle Ricerche, Istituto per la Microelettronica e Microsistemi (CNR-IMM), Catania, Italy | [4]Institute of Materials for Electronics and Magnetism, National Research Council (IMEM-CNR), Parma, Italy | [5]Department of Chemical Science, Life and Environmental Sustainability, University of Parma, Parma, Italy | [6]ATEN Center, University of Palermo, Palermo, Italy

Correspondence: Antonino Madonia (antonino.madonia@unipa.it)

Received: 10 September 2025 | **Revised:** 31 October 2025 | **Accepted:** 16 November 2025

Keywords: 2D materials | electron irradiation | MoS_2 | photoluminescence | Raman spectroscopy

ABSTRACT

Monolayer molybdenum disulfide is a semiconducting 2D material presenting very appealing characteristics for its incorporation into electronic flexible devices. At present, atomic vacancies in its structure are known to significantly affect its properties. Nonetheless, the effects of electron irradiation on it are still under investigation. In this work, the structural, electronic, and optical properties of monolayer molybdenum disulfide are studied before and after electron irradiation. By analyzing samples either obtained via a mechanical exfoliation process or grown via chemical vapor deposition, we show that following irradiation no significant change is present. This result indicates a strong resistance to the effect of electron irradiation at energies able to induce the formation of sulfur vacancies. By comparing our results to the current literature, we hypothesize that previously reported effects of electron irradiation are either due to the formation of molybdenum vacancies or to ionization of the electronic shell of this material. The presented results help to shed light on the role of atomic vacancies on the properties of this 2D material from a fundamental point of view and on its usage in extreme environment applications.

1 | Introduction

The interest in heterostructures based on Van der Waals materials has witnessed significant growth in recent years. Indeed, nowadays, a wide array of 2D materials presenting metallic, insulating, and semiconductor characteristics is available to researchers [1]. Such variety has led to the development of heterostructures composed of vertically stacked 2D covalent layers kept together by weak Van der Waals forces and interacting with their environment and substrate. Controllable stacking without the constraint of lattice matching has indeed allowed the development of prototype devices such as transistors [2], photodetectors [3], solar cells [4], and light-emitting diodes [5]. Among the many available 2D materials, transition metal dichalcogenides (TMDs) are renowned for their semiconducting electronic properties and tunable bandgap [6]. Molybdenum disulfide (MoS_2) in particular is considered an especially appealing TMD, because of its abundance in nature as a mineral and the ability to easily process it down to single 2D monolayers [7].

Although bulk MoS_2 is a semiconductor presenting an indirect bandgap of 1.2 eV, its properties are significantly affected by thickness. Indeed, it has been found that the states at the Γ point of its band structure are subjected to a strong interlayer coupling. When the thickness of MoS_2 is reduced down to a single layer, this coupling leads to a shift in the position of the minimum of

Emanuele Sangiorgi and Francesca Migliore contributed equally to this work.

the conduction band. In the monolayer case, such minimum is found at the K point of the Brillouin zone, so that direct transitions across the bandgap can be observed [8]. The recombination of photo-generated excitons thus leads to radiative transitions, absent in the case of multilayer MoS_2, responsible for an intense photoluminescence (PL) peaking approximately at 1.8 eV. Nowadays, monolayer MoS_2 (1L-MoS_2) is obtained following either top-down or bottom-up routes. Among the former, the gold-assisted exfoliation (GAE) method has been shown capable of yielding large-area flakes [9–11]. Although mechanical methods allow to obtain monolayers with unmatched structural and optical quality, the chemical vapor deposition (CVD) route is considered more appealing towards an industrial transfer [12, 13]. There is, indeed, a strong interest in incorporating the production of 1L-MoS_2 into the current fabrication procedures, facilitated by chemical synthetic pathways, with the intent of achieving flexible electronics integrating monolayer flakes. Such goal is realistically attainable considering the peculiar charge-transport properties of 1L-MoS_2, with a room-temperature mobility higher than $200\,cm^2\,V^{-1}\,s^{-1}$ [14], and surprising mechanical resistance and flexibility [15].

All of these characteristics have already led to the development of devices based on 1L-MoS_2 [16]. In such kind of devices, the monolayer flakes strongly interact with the underlying substrate, so that the final properties of the overall system are intimately linked to the characteristic of the whole heterostructure. Additionally, the performances of such devices are strongly connected to the quality of 1L-MoS_2 and the eventual presence of structural defects in the flakes can easily affect the final outcome [17]. Efforts have already been made towards tuning the properties of this material through mechanical [18] and chemical [19] modifications, thermal [20] and plasma [21] treatments, and by incorporating flakes into different dielectric environments [22, 23]. Although these strategies are viable during the production step, in view of using 1L-MoS_2 devices in real world applications, the effect of defect-inducing processes on this material has to be considered as well. Ionizing radiations are indeed well known to cause the formation of vacancies in 2D materials [24]. For devices used in extreme environments, such as solar cells in space, it is thus fundamental to know the effect of high-energy electrons on the structural properties of 1L-MoS_2 [25].

Electron irradiation was shown able to cause the formation of vacancies [26–28], alter the electronic properties of devices based on 1L-MoS_2 [29, 30], and change both the structural and optical properties of this material [31–33]. During this kind of irradiation, different processes can occur. In fact, the interactions between the electrons of the beam and those of the target induce excitation and ionization of the material's electronic shell, giving rise to the so-called ionizing dose effects [25]. Vacancy formation in such a case happens as a secondary process [24]. This process should be the only one present when the irradiation is performed with electrons having energies of few tens of keV. The exact cross-section depends on the irradiated sample's physical and chemical properties, so that its calculation often results challenging. On the other hand, at high energy (often in the hundreds of keV and MeV range), a direct knock-on causing atom displacement becomes probable too (displacement damage). Thresholds based on the formation energy of the different defects can in this case be used to selectively displace certain atoms. Depending on irradiation energy, the effects observed on the properties of 1L-MoS_2 can be selectively associated with sulfur vacancies, thus allowing us to understand their role in comparison to that of molybdenum vacancies. At present, the character of 1L-MoS_2 vacancies is still debated, with some works indicating that Mo and S ones introduce acceptor and donor levels in the energy band structure, respectively [34, 35]. Recent studies, on the other hand, indicate that S vacancies in 1L-MoS_2 cause a decrease in the concentration of negative charge carriers, thus giving them an acceptor character [36]. Finally, electron irradiation can also alter the properties of the substrate and other materials surrounding the 1L-MoS_2 flakes, either modifying their degree of interaction or directly worsening the quality of the electrical contacts in devices [29, 30]. Also, in such case, the characteristics of the whole heterostructure based on 1L-MoS_2 would significantly change due to the effect of irradiation.

In the present work, we explore the effect of high-energy electron irradiation on 2D MoS_2 trying at the same time to understand the role of atomic vacancies on its properties. By characterizing 1L-MoS_2 using micro-Raman and micro-PL spectroscopy, we intend to follow the changes to the structural, electronic, and optical properties of such material as a consequence of electron irradiation conducted at an energy of 0.5 MeV and fluences between $8 \times 10^{12}\,e^-\,cm^{-2}$ and $4 \times 10^{16}\,e^-\,cm^{-2}$. In these conditions, our calculations indicate that S vacancies are the most likely to form. Because of this, we can compare our results with a previous work conducted at 2.5 MeV, an energy at which both Mo and S vacancies are directly formed by knock-on processes [33], and pinpoint the role of different vacancies. Our results indicate 1L-MoS_2 to be resistant to the effects of electron irradiation conducted at the explored energy and suggest that the effects witnessed at higher energies are mostly due to Mo vacancies.

2 | Results and Discussion

The method used for the production of 1L-MoS_2 flakes can influence the structure of the obtained 2D material. Representative images obtained via optical microscopy with a 100× objective are shown in Figure 1 for 1L-MoS_2 grown via CVD on a SiO_2/Si substrate (Figure 1A) or obtained via GAE on Au/Ni/Si substrate (Figure 1B). The different contrast between the flakes and the substrate is due to the differences in refractive index between the monolayers and the material of the substrate, making 1L-MoS_2 almost transparent when deposited on the Au layer. Flakes grown by CVD result triangular in shape; indeed, the controlled 2D growth mostly proceeds in a diffusion-limited regime from the borders of 1L-MoS_2 flakes, leading to a distribution of crystalline monolayers sized between 5 μm and 25 μm (14 μm on average, $\sigma = 4$ μm) [37, 38]. Only for some larger flakes (approximately 30 μm), the growth of a second layer of 1L-MoS_2 is observed starting from the center (Figure S1). When considering 1L-MoS_2 flakes produced via the GAE method, larger monolayer regions with sides up to hundreds of microns can be obtained. Although high-quality monolayer regions are obtained [39], this production method does not provide any control on the thickness of the flakes and the exfoliation often leads to residual additional MoS_2 layers on top of the regions of interest (Figure S2). Despite the differences, both methods allow the study of wide isolated monolayer MoS_2 portions found within each sample.

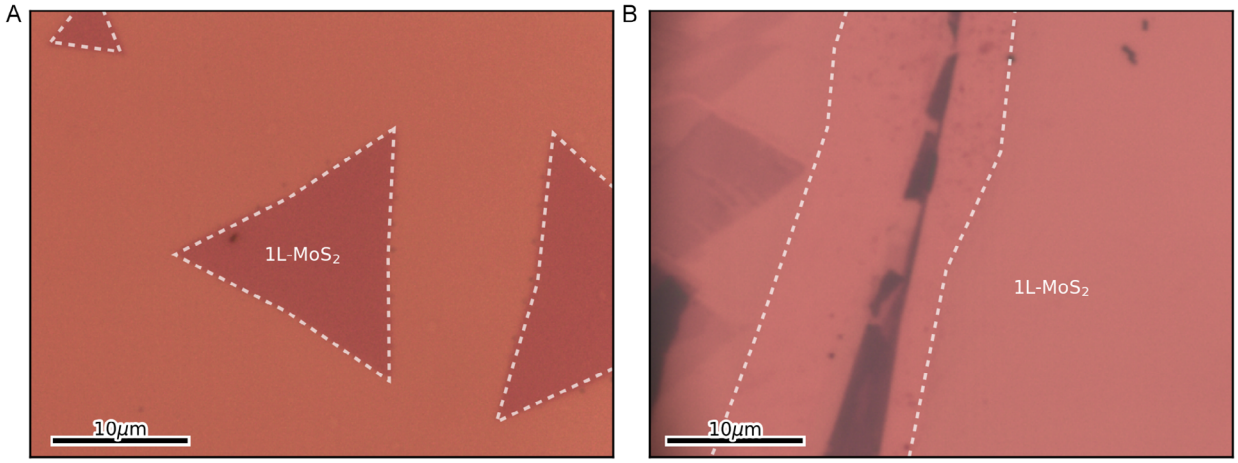

FIGURE 1 | Optical microscopy images of 1L-MoS_2 flakes grown by CVD (A) or obtained by GAE (B). The dashed lines indicate the contour of the flakes.

In order to study the effect of electron irradiation as a function of fluence, ten different samples, five grown via CVD and five obtained through GAE, were selected. For each sample, a 15 μm × 15 μm 1L-MoS_2 square region was characterized by Raman spectroscopy probing 100 points distributed across the surface at 1.5 μm steps. The results of the Raman characterization, which allow to study the electronic and structural properties of 1L-MoS_2 flakes, are shown in Figure 2. A typical 1L-MoS_2 Raman spectrum, as reported in Figure 2A, presents two main peaks at approximately 385 and 405 cm^{-1} associated with the in-plane E′ and out-of-plane A'_1 vibration of the material's lattice [40]. Two additional less intense bands were observed as well, located at approximately 375 and 450 cm^{-1} and associated with the longitudinal optical LO(M) and with the second-order longitudinal acoustic 2LA(M) vibrations respectively [41, 42]. The frequency and amplitude of the observed peaks were obtained by fitting each experimental spectrum with Lorentzian bands.

As shown in Figure 2B, the distance between the A'_1 and E′ peaks was found to be 17.8 cm^{-1} ($\sigma = 0.3\ cm^{-1}$) and 20.5 cm^{-1} ($\sigma = 0.4\ cm^{-1}$) for the flakes obtained by CVD and GAE, respectively. The distance between the two main 1L-MoS_2 Raman peaks confirms that the studied regions are indeed composed of monolayers; in fact, such frequency difference has been correlated to the thickness of MoS_2 and was found to be less than 22 cm^{-1} in the case of monolayers [43]. This difference is however found to be smaller in the case of flakes obtained via CVD and on insulating substrates [12, 44]. This effect, explaining the different distances found for CVD and GAE samples, stems from variations in the strain and doping of 1L-MoS_2, in turn affected by the flakes' substrate, local environment, and production method.

The strain and negative charge-carrier concentration can be obtained from the frequency of the Raman E′ and A'_1 peaks [45]. This method, detailed in the Supporting Information, allows to plot the strain-doping map shown in Figure 3. The map divides the plot into four quadrants related to 1L-MoS_2 under either compressive or tensile strain and presenting either negative or positive doping. From the plot, we can readily observe that all the studied flakes present an n-type doping, with a concentration of charge carriers on average equal to

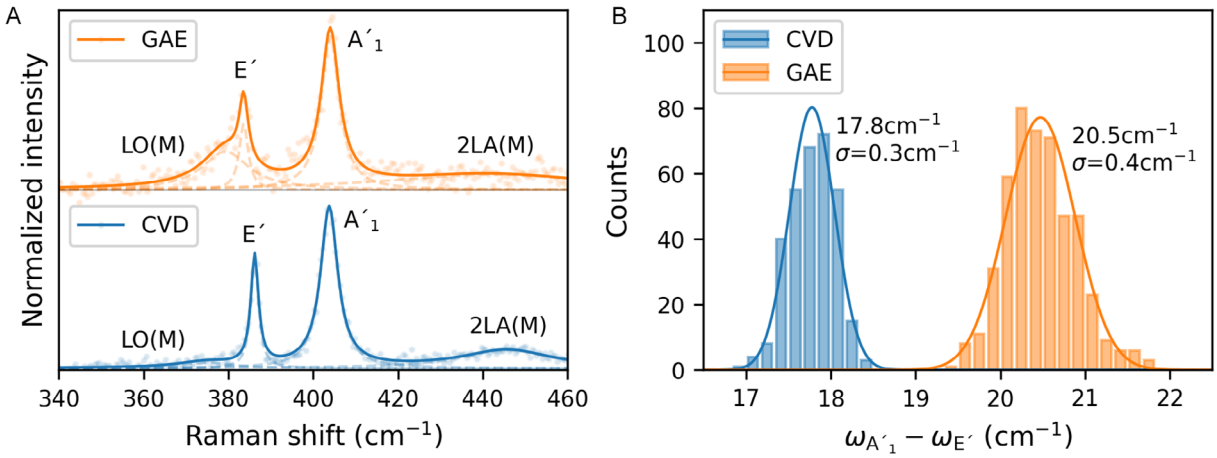

FIGURE 2 | (A) Normalized Raman spectra of 1L-MoS_2; experimental points are reported as semitransparent dots while the fitted spectra are reported as continuous lines; the Lorentzian peaks used to fit the experimental data are reported as dashed lines with labels indicating the corresponding vibration mode. (B) Histogram of the distances between the A'_1 and E′ Raman peaks' frequencies of 1L-MoS_2; the normal distribution fitting the data is reported as a continuous line whose center and standard deviation are reported as labels.

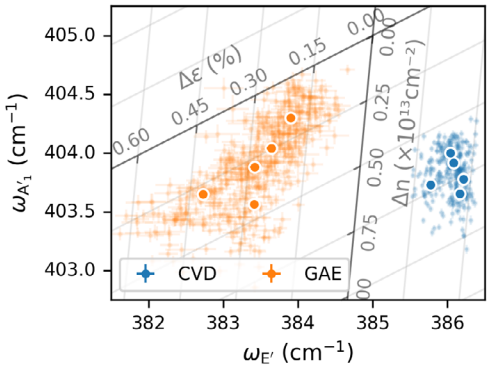

FIGURE 3 | Strain-doping map of 1L-MoS_2 obtained from the frequency of the A'_1 and E' Raman peaks; semitransparent dots represent the peaks' frequencies measured across the surface of several flakes while the larger dots indicate the average for each single flake.

$0.71 \times 10^{13}\,cm^{-2}$ ($\sigma = 0.02 \times 10^{13}\,cm^{-2}$) and to $0.28 \times 10^{13}\,cm^{-2}$ ($\sigma = 0.04 \times 10^{13} cm^{-2}$) for CVD and GAE samples, respectively. Additionally, while the CVD grown flakes present a compressive strain ($\varepsilon = -0.25\%$, $\sigma = 0.01\%$), the GAE samples are under a tensile strain condition ($\varepsilon = 0.29\%$, $\sigma = 0.03\%$). These results indicate that, compared to the GAE samples, the flakes grown via CVD show larger homogeneity in both strain condition and concentration of negative charge carriers.

The ten pristine samples were also characterized by means of photoluminescence (PL) spectroscopy to determine the characteristics of the photoemission of the studied 1L-MoS_2 flakes. For each sample, the same 15 μm × 15 μm 1L-MoS_2 surface previously characterized by Raman spectroscopy was analyzed. PL spectra were obtained at 49 different locations inside the probed square region at steps of 2 μm. The results of this characterization are shown in Figure 4, displaying normalized PL spectra representative of the two different kinds of samples. The observed photoemission is associated with the recombination of the A and B excitons. The two photo-excited excitons undergo a direct recombination from the conduction band to the valence band at the K point of the 1L-MoS_2; the difference in energy of the emission

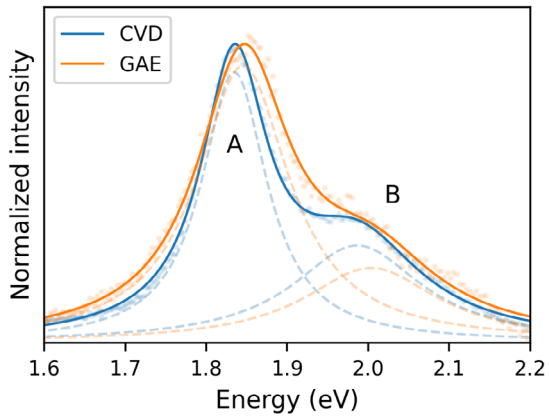

FIGURE 4 | Normalized PL spectra of 1L-MoS_2; experimental points are reported as semitransparent dots while the fitted spectra are reported as continuous lines; the Lorentzian peaks used to fit the experimental data are reported as dashed lines with labels indicating the corresponding excitonic recombination.

band associated to the two excitons is due to the valence band splitting caused by the spin–orbit interaction [8, 46].

The distribution of the PL amplitudes observed for the two different samples is shown in Figure 5A. The flakes obtained through the GAE method result in a more intense emission, with an amplitude on average equal to 284 a.u. ($\sigma = 70$ a.u.), compared to those grown via CVD which display an average amplitude equal to 229 a.u. ($\sigma = 28$ a.u.). Some studies have previously found that the presence of a Au substrate can quench the emission of 1L-MoS_2 due to an electron transfer mechanism [10, 39, 47]. On the other hand, similarly to our case, some studies observed that, by comparing the optical properties of 1L-MoS_2 flakes on different substrates, an increase in PL intensity can be witnessed on Au [48]. This result has been linked to the lower doping of the flakes deposited on Au compared to those on SiO_2. Since the optical properties of 1L-MoS_2 are strongly affected by the concentration of negative charge carriers in the flake [49], we hypothesize that the contrasting reports are due to differences in the electronic properties of the studied material.

As shown in Figure 5B, both kinds of samples present emission peaks located on average at very similar energies, with the A exciton band of the CVD sample (GAE sample) peaking at 1.84 eV (1.83 eV) and the B exciton band at 1.99 eV (1.98 eV). Nonetheless, the flakes obtained with the GAE method present a larger variability in the positions of both peaks, as attested by the standard deviations of their energy distribution ($\sigma = 0.02$ eV) which is four times larger than that obtained for CVD grown samples ($\sigma = 0.005$ eV). The PL intensity and shape of 1L-MoS_2 flakes can be strongly affected by applied mechanical strain as well as by the concentration of negative charge carriers [40, 49]. We hypothesize that the large variability in the characteristics of the PL spectra observed for GAE flakes is indeed due to the inhomogeneity in the strain and doping of the studied flakes [10]. In fact, the large distribution of the PL peaks' amplitude and energy mirrors the variability in the structural and electronic properties of 1L-MoS_2, found larger for GAE samples compared to the ones grown by CVD (Figure 3).

The effect of electron irradiation on 1L-MoS_2 was then studied at different fluences. The five characterized samples obtained with the two production methods were irradiated at the same electron energy, and the fluences were adjusted by exposing the samples to the beam for a longer duration. A beam energy of 0.5 MeV was selected by taking into consideration that the cross sections of the generation of Mo and S vacancies depend on it (Figure S3). At the chosen energy, the electrons can mostly cause displacement damage on S atoms, thus reducing the formation of Mo vacancies. This choice allows us to discern between the role of S and Mo vacancies and their effect on 1L-MoS_2 properties by comparing our study to experiments previously conducted at 2.5 MeV, since at this energy both atoms of the material are affected by displacement damage [33].

Following irradiation, the Raman and PL characterization were repeated on the same 1L-MoS_2 regions previously analyzed. Figure 6 shows the effects of irradiation on the properties as measured via Raman spectroscopy. Even after irradiation at the highest fluence of $4 \times 10^{16}\,e^{-}\,cm^{-2}$, the Raman spectra of both samples do not present any significant difference. Because of the variability of the Raman spectra within different portions of the same flake, the strain and concentration of negative charge carriers

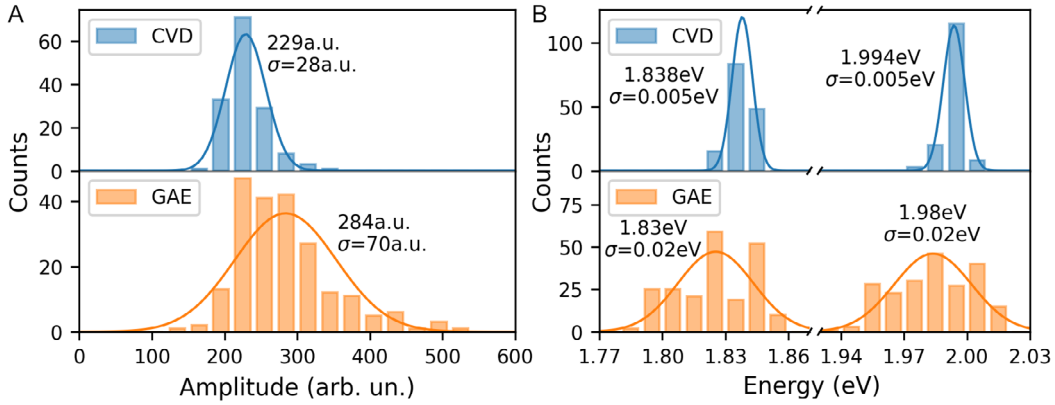

FIGURE 5 | Histograms of the total amplitude (A) and emission band energy (B) of the PL of 1L-MoS_2; the normal distribution fitting the data is reported as a continuous line whose center and standard deviation are reported as labels.

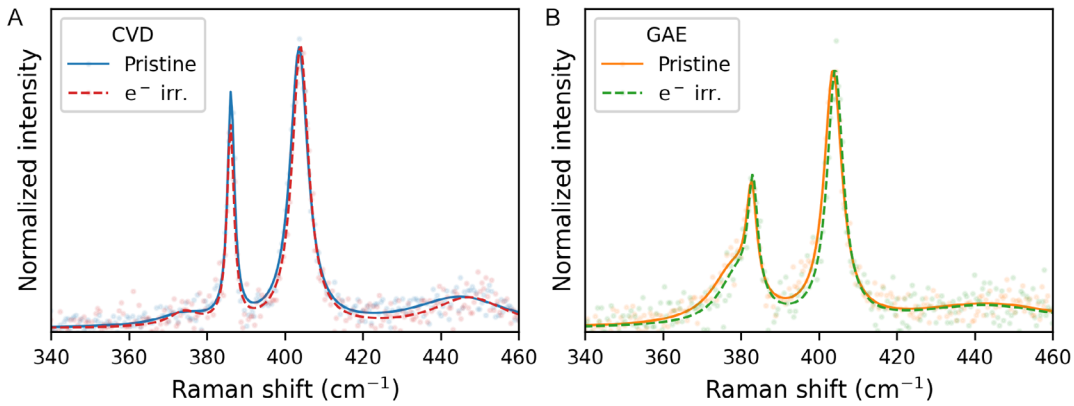

FIGURE 6 | Normalized Raman spectra of 1L-MoS_2 grown by CVD (A) or obtained by GAE (B) before and after irradiation at a fluence of $4 \times 10^{16}\,e^{-}\,cm^{-2}$; experimental points are reported as semitransparent dots while the fitted spectra are reported as continuous or dashed lines.

were calculated from the position of the E′ and A'_1 peaks of each spectrum and their distributions were compared to those obtained for pristine samples.

The variations in strain and in negative charge-carrier concentration as a function of fluence are reported in Figure 7A,B, respectively. These results clearly indicate that the electron irradiation has negligible effects on the structural and electronic properties of 1L-MoS_2 at the explored fluences. The observed differences in strain and concentration of negative charge carriers of the studied 1L-MoS_2 flakes are indeed found to be within 3σ of their variability regardless of irradiation fluence. An additional indication about the lack of structural modification to the irradiated 1L-MoS_2 flakes can be found in the amplitude of the 450 cm^{-1} 2LA(M) Raman peak. It has been reported that the amplitude of this band decreases as the concentration of defects in 1L-MoS_2 increases [41]. Nonetheless, as shown in Figure S4, the amplitude of this band does not vary with the fluence, suggesting that the performed irradiation does not lead to a significant defect formation in the studied material.

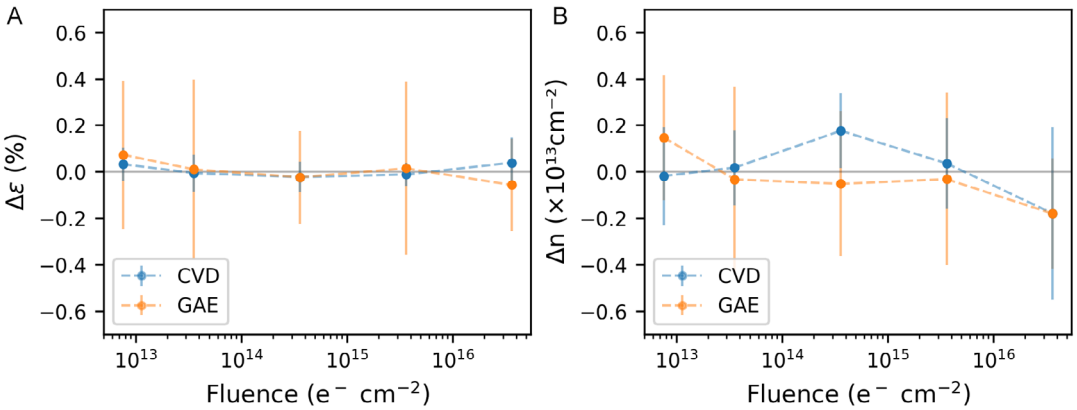

FIGURE 7 | Strain variation $\Delta\varepsilon$ (A) and negative charge-carrier concentration variation Δn (B) of 1L-MoS_2 as a function of irradiation fluence.

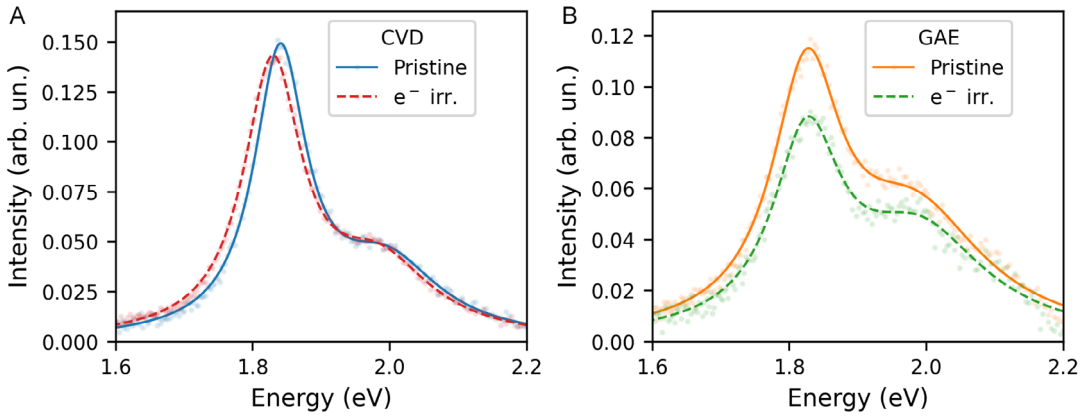

FIGURE 8 | PL spectra of 1L-MoS_2 grown by CVD (A) or obtained by GAE (B) before and after irradiation at a fluence of $4 \times 10^{16}\,e^-\,cm^{-2}$; experimental points are reported as semitransparent dots while the fitted spectra are reported as continuous or dashed lines.

Finally, the effects of the irradiation on the optical properties of 1L-MoS_2 are shown in Figure 8, displaying representative PL spectra obtained before and after irradiation at the highest fluence of $4 \times 10^{16}\,e^-cm^{-2}$. A slight decrease in the intensity of the bands is observed, especially for the emission spectrum of the flake obtained through GAE. At the same time, in the case of the CVD sample, the A exciton band presents a small decrease in emission energy and results redshifted compared to the spectrum before irradiation.

To analyze in detail the effect of irradiation on the optical properties, the variation of the PL amplitude and of the A exciton peak energy is plotted as a function of fluence in Figure 9A,B. When comparing the emission amplitude of the irradiated samples with respect to that before irradiation, we observe that the differences fall within 3σ of the inherent variability present across the probed 1L-MoS_2 flakes' surface. In fact, no obvious trend is found for both kinds of samples. When considering the energy of the emission bands, the same conclusion can be reached as their variations fall within the variability of the peaks' position found between different flakes. For instance, in the case of 1L-MoS_2 flakes grown by CVD at the highest fluence of $4 \times 10^{16}\,e^-cm^{-2}$, a redshift of 10 meV is observed. Despite this variation could appear to be significant, the A exciton peak position of CVD samples, as shown in Figure 5B, presents a standard deviation equal to 5 meV. Because of this, the apparent variation observed for the flake irradiated at the highest fluence cannot be considered significant at the 3σ level. This consideration can be applied to both bands of all the studied samples, as shown in Figure S5.

Overall, these results indicate that electron irradiation at an energy of 0.5 MeV and up to a fluence of $4 \times 10^{16}\,e^-cm^{-2}$ does not affect the optical properties of the studied 1L-MoS_2 samples. Considering that the PL properties are strongly influenced by strain and doping of the flakes [10, 40, 49], this result is not surprising. Indeed, no variations were found in the structural and electronic properties of the probed monolayers after irradiation, as shown in Figures 6 and 7.

The performed experiments show that irradiation with electrons at an energy of 0.5 MeV and fluences comparable to those encountered by a solar cell during space missions does not induce any significant modification in the structure of 1L-MoS_2, leaving its electronic and optical properties unvaried. Previous experiments conducted using electrons at lower energies were reported to strongly affect MoS_2 [27, 28]. The observed effects were associated with the displacement of sulfur atoms and with the formation of vacancies caused by the electron beam [26]. However, the irradiations were performed under flux and fluence values much higher than those used for our experiments. Moreover, the low beam energies imply higher stopping power values which further increase the dose rate and the total dose, so that the ionizing mechanism could still be dominant [27].

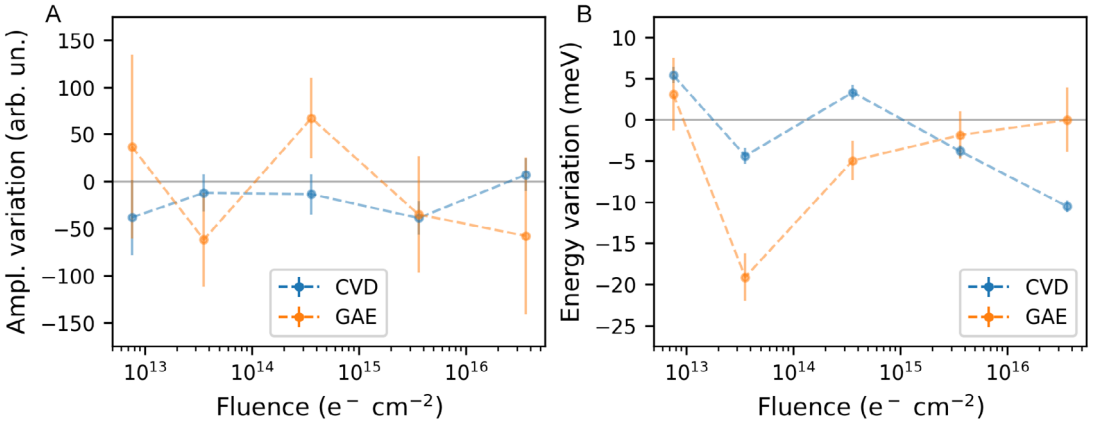

FIGURE 9 | Total amplitude variation (A) and A emission band energy variation (B) of the PL of 1L-MoS_2 as a function of irradiation fluence.

Other studies demonstrated changes in the electronic performances of FETs and memory devices based on 1L-MoS_2. Although modifications to the optical properties of 1L-MoS_2 were not always witnessed [30], the conducted studies were able to observe changes in the structural and electronic properties of the material, as witnessed by changes in the Raman spectra, and a decrease in the output current of the analyzed device [30, 32]. Also, in this case, sulfur vacancies were found and blamed to be the underlying cause for the decrease in electronic performance. Nonetheless, other studies indicate that electron irradiation could improve the performance of transistors incorporating 1L-MoS_2 [29] and improve its PL [31]. In these cases, it was hypothesized that the irradiation effects were caused by interfacial reactions such as the atomic diffusion at the metal contacts of the device and oxidation of MoS_2.

The type of mechanism taking place during the interaction between the electrons and the atoms of 1L-MoS_2 depends on the energy of the irradiation beam. In order for a knock-on displacement of an atom to occur following a collision, the electron of the beam must be able to transfer to the atom an energy higher than a threshold value related to the vacancy formation energy of that atom in the material. Otherwise, only ionization processes due to interactions between the electrons of the beam with those of the shell of the material's atoms can occur [50]. As consequence, while the latter are always present, the displacement ones can be activated by changing the energy of the beam. The kinetic energy threshold of the beam electrons needed for a displacement damage event and the formation of a vacancy can be calculated by considering the energy transferred during an electron-nucleus collision [51]. In the case of 1L-MoS_2, the formation energies of sulfur and molybdenum vacancies have been calculated to be equal to 6.1 and 13.9 eV, respectively [52]. By taking these values into consideration, as explained in the Supporting Information, thresholds below 100 keV and at about 400 keV are obtained for the formation of chalcogen and metal atom vacancies, respectively. Below these values, no vacancy can be formed by knock-on, while other mechanisms must be taken into account. Indeed, soft collisions can cause effects such as excitation or ionization of the atom, then leading to the generation of a vacancy as a secondary process [24].

The electron beam energy used in our experiments is high enough that the formation of vacancies can be considered due to knock-on collisions and that sulfur vacancies are the main type of defect expected by electron irradiation. Indeed, molybdenum vacancies would be generated in a very small number since the used energies are just above the threshold needed for their formation. At higher energies, instead, both sulfur and molybdenum vacancies are formed, as shown in Figure S3. Studies conducted with 1 MeV electrons in ambient atmosphere (while our irradiations were performed under He atmosphere) have shown the modification of the Raman and PL bands of 1L-MoS_2 associated with vacancy formation and MoS_2 oxidation [30, 31]. Another study conducted by our group at 2.5 MeV was able to witness a decrease in the intensity and a redshift in the position of the PL of 1L-MoS_2 [33]. By considering the higher energies involved in that experiment, we conclude that both sulfur and molybdenum vacancies must have formed and that the total concentration of defects is therefore higher. By using the data of the simulation reported in Figure S3, we can estimate that at 2.5 MeV, there are about 4 times more defects related to S and Mo vacancies. In the 2.5 MeV experiments, a relevant difference in the PL intensity was observed already at a fluence of about $4 \times 10^{14}\,e^{-}\,cm^{-2}$, a value that is two orders of magnitude lower than the maximum fluence used for the irradiation at 0.5 MeV. Being this difference larger than the factor 4 in defect concentration, we can suggest that the origin of variations of the PL signal in the 2.5 MeV irradiated samples is related to the larger amount of Mo vacancies. By contrast, in the reported experiment, the explored conditions only allow for the formation of sulfur vacancies, and they did not yield any significant change in the structural, electronic, and optical properties of 1L-MoS_2. This result suggests that, differently to what discussed in the literature, sulfur vacancies either have a smaller role on the properties of 1L-MoS_2 or they are less stable in our samples. Overall, the lack of effects on either the structural or optical properties indicates that the effect of irradiation on 1L-MoS_2 should be explored in more detail. Our analysis has shown a remarkable resistance of this monolayer material to the effects of electron irradiation at 0.5 MeV and a good resistance at 2.5 MeV [32], especially in terms of structural and electrical properties in a range of fluences up to $4 \times 10^{16}\,e^{-}\,cm^{-2}$ (which roughly corresponds to about 10^4 kGy in both cases). Although measurements of the electrical properties of the studied 1L-MoS_2 would result in a more direct proof of its resistance to the effects of irradiation, performing such experiments requires the deposition of electrical contacts on top of small sized flakes. As discussed in the literature, electron irradiation can, in some cases, alter the quality of such contacts [29, 30], thus changing the properties of the device without, in line of principle, influencing the 1L-MoS_2 flakes. The performed statistical analysis of the spectroscopic characteristics of the studied monolayer flakes, on the other hand, is not affected by such aspect and has been used in previous investigations to characterize the sign and the concentrations of the free carriers [44, 45, 53]. Finally, further analysis conducted as a function of irradiation energy would give additional insight into the formation mechanisms and threshold energies of Mo and S vacancies, helping to clarify their role on the properties of 1L-MoS_2.

3 | Conclusion

Monolayer MoS_2 flakes obtained via two different methods were characterized before and after high-energy electron irradiation. The methods used for preparing the studied flakes are representative of the most common approaches for the production of 1L-MoS_2, consisting in the mechanical top-down exfoliation method assisted by gold substrate and the bottom-up chemical vapor deposition. By means of Raman spectroscopy, the structural and electronic properties of the analyzed 2D material were studied and statistically investigated for a set of five different flakes for each production method. It was found that mechanical exfoliation samples present a tensile strain in their structure, while samples obtained via the chemical route display a compressive strain. Additionally, a higher concentration of negative charge carriers was found in the case of CVD grown samples, compared to those obtained via GAE. In general, gold exfoliation resulted in MoS_2 flakes presenting more inhomogeneous properties. Moreover, the optical properties of our samples were also studied by means of PL spectroscopy, once again analyzing the amplitude and energy distributions of the photoemission generated by the same ten flakes. Although slightly, 1L-MoS_2

produced via mechanical exfoliation displayed a stronger emission intensity. At the same time, the energy distribution of the observed PL bands resulted comparable for both kinds of samples. Once again, a larger inhomogeneity was displayed by the optical properties of GAE samples, in line with the Raman characterization results. After irradiating the studied samples with 0.5 MeV electrons, no significant changes were found in any of their properties regardless on the used substrate and preparation route. At the electron beam energy used for our experiments, sulfur vacancies are the defects most likely to form by displacement damage mechanism. This consideration allows us to hypothesize that, when the used irradiation beam consists of low-energy electrons, the effects of irradiation on monolayer MoS_2 discussed in the literature are caused by excitation and ionization mechanisms happening because of soft collisions. In the case of experiments conducted at higher energy, considering that a consistent number of molybdenum vacancies should be formed above 0.5 MeV, we can suggest that the witnessed effects should be due to Mo vacancies and that, as a consequence, limiting their generation is of primary relevance to improve radiation hardness. The lack of changes in samples irradiated at 0.5 MeV in which sulfur vacancies should be induced is in line with recent works indicating that the negative doping character of 1L-MoS_2 is not due to this kind of defect [36]. Finally, electron irradiation should be studied in more detail in order to reach a conclusive understanding of its effect. Such experiments would yield important knowledge regarding the usage of devices based on 1L-MoS_2 for extreme-environment applications. By testing that such material is resistant to the effects of electron irradiation, we are proving that 1L-MoS_2 could guarantee long-lasting energy production when used for satellite-mounted solar cells. Additionally, by carefully studying the electron energy dependence of such effect, the role of Mo and S vacancies on the properties of monolayer MoS_2 could be better understood from a fundamental point of view.

4 | Experimental Methods

4.1 | Preparation of GAE Samples

The samples' substrate are obtained by sputtering a film of Ni (10 nm) and of Au (10 nm) on top of SiO_2 (900 nm)/Si using a DC magnetron sputtering in a Q300T D PLUS system (Quorum Technologies, Laughton, United Kingdom), as described in previous publications [44]. Pressure was maintained at a maximum of 10^{-2} mbar during the sputtering. A bulk MoS_2 stamp obtained from a freshly cleaved 2H-MoS_2 crystal was then pressed against the substrates. The pressing onto the substrate step was carried out immediately after the sputtering procedure to prevent contamination of the surface.

4.2 | Preparation of CVD Samples

The samples were prepared by Liquid-Precursors-Intermediated Chemical Vapour Deposition (LPI-CVD) at 820°C under sulfur vapor flux, using as Mo precursor a spin-coated solution of ammonium heptamolybdate tetrahydrate (AHT, Sigma–Aldrich, 99.98%) 0.003 mol/L, sodium idroxide (NaOH) 0.060 mol/L, and OptiPrepTM (a solution of 60% (w/v) iodixanol in water, with a concentration of 0.5 ml for 5 ml). The CVD growth was carried out in an open tube with nitrogen as the carrier gas. Further details can be found in references [38, 54, 55]. The used substrates were 290 nm thick SiO_2 coated silicon wafers.

4.3 | Sample Characterization

Structural, electronic, and optical properties of 1L-MoS_2 were studied via Micro-Raman and micro-PL spectroscopy using a LabRam HR-Evolution Spectrometer system (HORIBA France SAS, Lyon, France) coupled to a confocal microscope with a pinhole of 200 μm and a 100× objective. A laser excitation source with a wavelength of 532 nm was used to record all spectra. Laser power was reduced to 1% or 5% of the 100 mW maximum using an ND filter, for CVD and GAE samples, respectively. 1800 lines/mm and 600 lines/mm gratings were used to acquire Raman data and PL spectra, respectively. All spectra were collected across a 15×15 μm^2 area, with a step size of 1.5 and 2 μm for Raman and PL measurements, respectively. Reported values calculated from the Raman and PL spectra correspond to the average of all the different measurements acquired across the relevant areas. The Raman peak at 520.70 cm^{-1} arising from the Si present in the samples' substrate was used for Raman spectral calibration. The integrated Raman bands of 1L-MoS_2 have been used to normalize the PL bands intensity to take into account excitation instabilities and differences in focus position of the microscope objective. Spectral bands were fitted with Lorentzian-shaped peaks. All reported uncertainties correspond to three times the standard deviation.

4.4 | Irradiation Experiments

Electron irradiation was carried out with a Pelletron accelerator at Sirius facility (LSI, France) exploring the fluence range $8 \times 10^{12}\,e^{-}\,cm^{-2}$ up to $4 \times 10^{16}\,e^{-}\,cm^{-2}$ at room temperature (approximately 25°C) and under a 0.4 mbar He atmosphere. Electron beam energy was fixed at 0.5 MeV. Beam diameter was equal to 20 mm, and a current of 0.1 μA was used for the lowest fluence while 1 μA for all other fluences. Total fluence was changed by selecting the duration of irradiation.

Acknowledgments

This research was funded by the Italian MUR PNRR project SAMOTHRACE (ECS00000022) and the PRIN 2022 project titled 2D materials Integration with Nitride semiconductors for advanced Electronics (2DIntegratE) (2022RHRZN2) under the National Recovery and Resilience Plan (NRRP), Mission 4, Component 2, Investment 1.1, Call for tender No. 104 published on 2.2.2022 by the Italian Ministry of University and Research (MUR), funded by the European Union—NextGenerationEU. L.S and F.E. (IMEM-CNR) wish to acknowledge the help of Dr. Giovanni Attolini and Dr. Matteo Bosi in carrying out the CVD growth of MoS_2.

Open access publishing facilitated by Universita degli Studi di Palermo, as part of the Wiley - CRUI-CARE agreement.

Funding

The work was supported by Ministero dell'Università e della Ricerca (Grants ECS00000022 and 2022RHRZN2) and European Union.

Conflicts of Interest

The authors declare no conflicts of interest.

Data Availability Statement

The data that support the findings of this study are available from the corresponding author upon reasonable request.

References

1. A. K. Geim and I. V. Grigorieva, "Van der Waals Heterostructures," *Nature* 499 (2013): 419, https://doi.org/10.1038/nature12385.

2. L. Liao, J. Bai, Y. Qu et al., "High-κ Oxide Nanoribbons as Gate Dielectrics for High Mobility Top-Gated Graphene Transistors," *Proceedings of the National Academy of Sciences* 107 (2010): 6711, https://doi.org/10.1073/pnas.0914117107.

3. R.-J. Shiue, Y. Gao, Y. Wang, et al., "High-Responsivity Graphene–Boron Nitride Photodetector and Autocorrelator in a Silicon Photonic Integrated Circuit," *Nano Letters* 15 (2015): 7288, https://doi.org/10.1021/acs.nanolett.5b02368.

4. M. Massicotte, P. Schmidt, F. Vialla, et al., "Picosecond Photoresponse in Van der Waals Heterostructures," *Nature Nanotechnology* 11 (2016): 42–46, https://doi.org/10.1038/nnano.2015.227.

5. F. Withers, O. Del Pozo-Zamudio, A. Mishchenko et al., "Light-Emitting Diodes by Band-Structure Engineering in Van der Waals Heterostructures," *Nature Materials* 14 (2015): 301, https://doi.org/10.1038/nmat4205.

6. Y. Liu, N. O. Weiss, H. C. Duan et al., "Van der Waals Heterostructures and Devices," *Nature Reviews Materials* 1 (2016): 1–7, https://doi.org/10.1038/natrevmats.2016.42.

7. I. Song, C. Park, H. C. Choi, "Synthesis and Properties of Molybdenum Disulphide: From Bulk to Atomic Layers," *RSC Advances* 5 (2015): 7495–514, https://doi.org/10.1039/C4RA11852A.

8. A. Splendiani, L. Sun, Y. Zhang, et al., "Emerging Photoluminescence in Monolayer MoS_2," *Nano Letters* 10 (2010): 1271, https://doi.org/10.1021/nl903868w.

9. S. E. Panasci, E. Schilirò, F. Roccaforte, et al., "Gold-Assisted Exfoliation of Large-Area Monolayer Transition Metal Dichalcogenides: From Interface Properties to Device Applications," *Advanced Functional Materials* 35 (2025): 2414532, https://doi.org/10.1002/adfm.202414532.

10. M. Velický, G. E. Donnelly, W. R. Hendren, et al., "Mechanism of Gold-Assisted Exfoliation of Centimeter-Sized Transition-Metal Dichalcogenide Monolayers," *ACS Nano* 12 (2018): 10463, https://doi.org/10.1021/acsnano.8b06101.

11. S. B. Desai, S. R. Madhyapathy, M. Amani, et al., "Gold-Mediated Exfoliation of Ultralarge Optoelectronically-Perfect Monolayers," *Advanced Materials* 28 (2016): 4053, https://doi.org/10.1002/adma.201506171.

12. Y. Zhan, et al., "Large-Area Vapor-Phase Growth and Characterization of MoS_2 Atomic Layers on a SiO2 Substrate," *Small* (2012), https://doi.org/10.1002/smll.201102654.

13. A. Tonon, E. Di Russo, F. Sgarbossa, et al., "Laser Induced Crystallization of Sputtered MoS_2 Thin Films," *Materials Science in Semiconductor Processing* 164 (2023): 107616, https://doi.org/10.1016/j.mssp.2023.107616.

14. B. Radisavljevic, A. Radenovic, J. Brivio, et al., "Single-Layer MoS_2 Transistors," *Nature Nanotechnology* 6 (2011): 147, https://doi.org/10.1038/nnano.2010.279.

15. R. C. Cooper, C. Lee, C. A. Marianetti, et al., "Nonlinear Elastic Behavior of Two-Dimensional Molybdenum Disulfide," *Physical Review B* 87 (2013): 035423, https://doi.org/10.1103/PhysRevB.87.035423.

16. H. Singh Nalwa, "A Review of Molybdenum Disulfide (MoS_2) Based Photodetectors: From Ultra-Broadband, Self-Powered to Flexible Devices," *RSC Advances* 10 (2020): 30529, https://doi.org/10.1039/D0RA03183F.

17. J. Jiang, P. Yang, J. J. Liou, W. Liao, and Y. Chai, "Defect Engineering of Two-Dimensional Materials towards Next-Generation Electronics and Optoelectronics," *Nano Research* 16 (2023): 3104, https://doi.org/10.1007/s12274-022-5016-9.

18. K. He, C. Poole, K. F. Mark, and J. Shan et al., "Experimental Demonstration of Continuous Electronic Structure Tuning via Strain in Atomically Thin MoS_2," *Nano Letters* 13 (2013): 2931, https://doi.org/10.1021/nl4013166.

19. J. Seo, E. Son, J. Kim, S. W. Kim, J. M. Baik, and H. Park, "Controllable Substitutional Vanadium Doping in Wafer-Scale Molybdenum Disulfide Films," *Nano Research* 16 (2023): 3415, https://doi.org/10.1007/s12274-022-4945-7.

20. E. Sangiorgi, A. Madonia, G. Laurella, et al., "Mild Temperature Thermal Treatments of Gold-Exfoliated Monolayer MoS_2," *Nanomaterials* 15 (2025): 160, https://doi.org/10.3390/nano15030160.

21. R. G. Costa, A. do Nascimento Barbosa, M. E. da Costa, et al., "Resonance Raman Spectroscopy of MoS_2 Monolayers Treated with Nitrogen Plasma," *Vibrational Spectroscopy* 123 (2022): 103454, https://doi.org/10.1016/j.vibspec.2022.103454.

22. Y. Lin, X. Ling, L. Lu, et al., "Dielectric Screening of Excitons and Trions in Single-Layer MoS_2," *Nano Letters* 14 (2014): 5569, https://doi.org/10.1021/nl501988y.

23. J. Ryou, et al., "Monolayer MoS_2 Bandgap Modulation by Dielectric Environments and Tunable Bandgap Transistors," *Scientific Reports* (2016), https://doi.org/10.1038/srep29184.

24. L. Sun, ed. In-Situ Transmission Electron Microscopy (Springer Nature Singapore, (2023).

25. A. Alessi, et al., "Electron Irradiation: From Test to Material Tailoring," *Europhysics Letters* (2023), https://doi.org/10.1209/0295-5075/acf47c.

26. H.-P. Komsa, et al., "Two-Dimensional Transition Metal Dichalcogenides under Electron Irradiation: Defect Production and Doping," *Physical Review Letters* (2012), https://doi.org/10.1103/PhysRevLett.109.035503.

27. R. Zan, et al., "Control of Radiation Damage in MoS_2 by Graphene Encapsulation," *ACS Nano* (2013), https://doi.org/10.1021/nn4044035.

28. W. M. Parkin, et al., "Raman Shifts in Electron-Irradiated Monolayer MoS_2," *ACS Nano* (2016), https://doi.org/10.1021/acsnano.5b07388.

29. A. Pelella, et al., "Electron Irradiation of Metal Contacts in Monolayer MoS_2 Field-Effect Transistors," *ACS Applied Materials & Interfaces* (2020), https://doi.org/10.1021/acsami.0c11933.

30. H. Li, et al., "Electron Radiation Effects on the Structural and Electrical Properties of MoS_2 Field Effect Transistors," *Nanotechnology* (2019), https://doi.org/10.1088/1361-6528/ab3ce2.

31. H. Li, et al., "Modulation of 1 MeV Electron Irradiation on Ultraviolet Response in MoS_2FET," *Nanotechnology* (2021), https://doi.org/10.1088/1361-6528/ac1d79.

32. X. Wu, et al., "Electron Irradiation-Induced Defects for Reliability Improvement in Monolayer MoS_2-Based Conductive-Point Memory Devices, "*Npj 2D Materials and Applications* (2022), https://doi.org/10.1038/s41699-022-00306-8.

33. S. E. Panasci, et al., "Electron Irradiation Effects on Single-Layer MoS_2 Obtained by Gold-Assisted Exfoliation," *Physica Status Solidi (a)* (2022), https://doi.org/10.1002/pssa.202200096

34. H. Qiu, et al., "Hopping Transport through Defect-Induced Localized States in Molybdenum Disulphide," *Nature Communications* (2013), https://doi.org/10.1038/ncomms3642.

35. L. Feng, et al., "Effect of Vacancies on Structural, Electronic and Optical Properties of Monolayer MoS_2: A First-Principles Study," *Journal of Alloys and Compounds* (2014), https://doi.org/10.1016/j.jallcom.2014.06.018.

36. Y. Park, et al., "Unveiling the Origin of n-Type Doping of Natural MoS_2: Carbon," *Npj 2D Materials and Applications* (2023), https://doi.org/10.1038/s41699-023-00424-x.

37. L. Seravalli, et al., "Built-in Tensile Strain Dependence on the Lateral Size of Monolayer MoS_2 Synthesized by Liquid Precursor Chemical Vapor Deposition," *Nanoscale* (2023), https://doi.org/10.1039/D3NR01687K.

38. F. Esposito, et al., "Role of Density Gradients in the Growth Dynamics of 2-Dimensional MoS_2 Using Liquid Phase Molybdenum Precursor in Chemical Vapor Deposition," *Applied Surface Science* (2023), https://doi.org/10.1016/j.apsusc.2023.158230.

39. S. E. Panasci, et al., "Substrate Impact on the Thickness Dependence of Vibrational and Optical Properties of Large Area MoS_2 Produced by Gold-Assisted Exfoliation," *Applied Physics Letters* (2021), https://doi.org/10.1063/5.0062106.

40. D. Lloyd, et al., "Band Gap Engineering with Ultralarge Biaxial Strains in Suspended Monolayer MoS_2," *Nano Letters* (2016), https://doi.org/10.1021/acs.nanolett.6b02615.

41. S. Mignuzzi, A. J. Pollard, N. Bonini et al., "Effect of Disorder on Raman Scattering of Single-Layer MoS_2," *Physical Review B* 91 (2015): 195411, https://doi.org/10.1103/PhysRevB.91.195411.

42. B. R. Carvalho, Y. Wang, S. Mignuzzi et al., "Intervalley Scattering by Acoustic Phonons in Two-Dimensional MoS_2 Revealed by Double-Resonance Raman Spectroscopy," *Nature Communications* 8 (2017): 14670, https://doi.org/10.1038/ncomms14670.

43. C. Lee, H. Yan, L. E. Brus et al., "Anomalous Lattice Vibrations of Single- and Few-Layer MoS," *ACS Nano* 4 (2010): 2695–700, https://doi.org/10.1021/nn1003937.

44. S. E. Panasci, E. Schiliroò, G. Greco et al., "Strain, Doping, and Electronic Transport of Large Area Monolayer MoS_2 Exfoliated on Gold and Transferred to an Insulating Substrate," *ACS Applied Materials & Interfaces* 13 (2021): 31248, https://doi.org/10.1021/acsami.1c05185.

45. A. Michail, et al., "Optical Detection of Strain and Doping Inhomogeneities in Single Layer MoS_2," *Applied Physics Letters* (2016), https://doi.org/10.1063/1.4948357.

46. Z. Y. Zhu, Y. C. Cheng, U. Schwingenschlögl et al., "Giant Spin-Orbit-Induced Spin Splitting in Two-Dimensional Transition-Metal Dichalcogenide Semiconductors," *Physical Review B* 11 (2011): 153402, https://doi.org/10.1103/PhysRevB.84.153402.

47. U. Bhanu, M. R. Islam, L. Tetard et al., "Photoluminescence Quenching in Gold - MoS_2 Hybrid Nanoflakes," *Scientific Reports* 4 (2014): 5575, https://doi.org/10.1038/srep05575.

48. M. Buscema, G. A. Steele, H. S. J. Van Der Zant et al., "The Effect of the Substrate on the Raman and Photoluminescence Emission of Single-Layer MoS_2," *Nano Research* 4 (2014): 561, https://doi.org/10.1007/s12274-014-0424-0.

49. B. Chakraborty, A. Bera, D. V. S. Muthu et al., "Symmetry-Dependent Phonon Renormalization in Monolayer MoS_2 Transistor," *Physical Review B* 85 (2012): 161403, https://doi.org/10.1103/PhysRevB.85.161403.

50. F. Banhart, "Irradiation Effects in Carbon Nanostructures," *Reports on Progress in Physics* 62 (1999): 1181, https://doi.org/10.1088/0034-4885/62/8/201.

51. L. Reimer, Transmission Electron Microscopy: Physics of Image Formation and Microanalysis (Springer Berlin Heidelberg, (1989).

52. X. Liu, T. Xu, X. Wu et al., "Top–down Fabrication of Sub-Nanometre Semiconducting Nanoribbons Derived From Molybdenum Disulfide Sheets," *Nature Communications* (2013), https://doi.org/10.1038/ncomms2803.

53. S. E. Panasci, E. Schilirò, G. Greco et al., "Impact of the Schottky Barrier and Contact-Induced Strain Variations inside the Channel on the Electrical Behavior of Monolayer MoS_2 Transistors," *Small Science* (2025), https://doi.org/10.1002/smsc.202500244.

54. L. Seravalli, M. Bosi, P. Fiorenza et al., "Gold Nanoparticle Assisted Synthesis of MoS_2 Monolayers by Chemical Vapor Deposition," *Nanoscale Advances* 3 (2021): 4826, https://doi.org/10.1039/D1NA00367D.

55. F. Esposito, M. Bosi, G. Attolini et al., "Influence of the Carrier Gas Flow in the CVD Synthesis of 2-Dimensional MoS_2 Based on the Spin-Coating of Liquid Molybdenum Precursors," *Nanomaterials* 14 (2024): 1749, https://doi.org/10.3390/nano14211749.

Supporting Information

Additional supporting information can be found online in the Supporting Information section. **Supporting Fig. S1:** Optical microscopy image obtained with a 10× objective of 1L-MoS_2 flakes grown by CVD. Scale bar corresponds to 20 μm. **Supporting Fig. S2:** Optical microscopy image obtained with a 10× objective of 1L-MoS_2 flakes obtained by GAE. Scale bar corresponds to 20 μm. **Supporting Fig. S3:** SECTE[S4] simulated cross-sections for Mo and S vacancy production as a function of electron beam energy, displacement threshold energy 6.1 and 13.9 eV for S and Morespectively. **Supporting Fig. S4:** Variation with respect to the not irradiated sample of the amplitude of the 2LA(M) Raman peak of 1L-MoS_2 grown by CVD (A) or obtained by GAE (B) as a function of irradiation fluence. **Supporting Fig. S5:** Variation of the B emission band energy of the PL of 1L-MoS_2 grown by CVD (A) or obtained by GAE (B) as a function of irradiation fluence.